Cooperative ridge-trench formation in heteroepitaxial systems

Zhijun Huang, Tianze Zhou, and Cheng-hsin Chiu*
Department of Materials Science and Engineering, National University of Singapore, Singapore 117576, Singapore
(Received 21 May 2007; published 22 October 2007)

In this paper we investigate the cooperative ridge-trench formation from the theoretical point of view. Our investigation starts with numerical simulation for the morphological evolution of strained film-substrate system driven by surface diffusion. The results demonstrate that the morphological evolution of thick films leads to the unique cooperative formation of faceted trenches and ridges. The cooperative formation is further analyzed from the energy point of view by considering the two pathways of the cooperative formation, namely, the growth of the outermost structure and the gradual formation of a faceted structure adjacent to the existing one. The analyses reveal that the first pathway dictates the process initially, while the second one is more energetically favorable once the size of the outermost structure reaches a critical value. The competition of the two pathways repeats, resulting in the cooperative ridge-trench formation.

DOI: 10.1103/PhysRevB.76.155426 PACS number(s): 68.35.Fx, 68.55.−a, 81.16.Dn

I. INTRODUCTION

Rippling on solid surfaces at the length scale of nanometers is a remarkable phenomenon of self-assembly. The phenomenon was observed in Ref. 1 by annealing a $Si_{0.5}Ge_{0.5}$ alloy film of 5 nm in thickness on a thick Si substrate at temperatures ranging from 570 to 590 °C. The result revealed that the film developed into nanoridges and nanotrenches via a cooperative manner that the two types of nanostructures formed one after another at the adjacent sites. The cooperative ridge-trench (CRT) formation continued, resulting in a ripple structure. The ripples were characterized by the same type of facet but could exhibit a variety of different shapes. Similar ripple structures were also found in other SiGe films[2,3] and in the InGaAs/GaAs system.[4,5]

Subsequent to the observation in Ref. 1, the CRT formation was realized to be a useful mechanism for self-assembling quantum-dot molecules (QDMs) on heteroepitaxial systems.[6] The fabrication process of the QDMs consisted of two steps. The first step was to generate shallow holes on solid surfaces by embedding a small amount of hard particles in a buffer layer prior to the deposition of a heteroepitaxial film.[6–8] The shallow holes would trigger the CRT formation on the film in the second step, causing the self-assembly of QDMs around the holes. The QDMs generated by this process were clusters of dots with the number of dots being adjustable.[9] The size distribution of the QDMs was much more uniform than that of single quantum dots. These advantages, namely, self-assembly, unique structures, adjustable number of dots, and uniform size distribution, suggest that the QDMs are a promising building block for quantum computation devices.[10]

In addition to the two situations mentioned above,[1,6] the CRT formation also happened on heteroepitaxial films during the deposition process. This issue was examined in a series of papers aiming at understanding the dependence of the CRT formation on the growth rate, the substrate temperature, the film thickness, and the interrupting annealing during the process.[11–16] Those papers focused on the $Si_{0.7}Ge_{0.3}$/Si system, and the key findings can be summarized as follows. (1) At 550 °C and a growth rate of 0.09 nm/s, the film morphology developed shallow indents and then QDMs via the CRT formation.[11] The QDMs were mainly quantum fortresses, characterized by a {105} ring surrounding a square pit with the same type of facet. (2) At the same 550 °C but a much slower growth rate (0.015 nm/s), no shallow indent was found, and the film morphological evolution led to a ripple structure when the film thickness reached 30 nm.[11] The ripple structure was similar to that observed in Ref. 1. (3) Increasing the temperature to 750 °C with similarly low growth rates caused nanoislands to form at small thickness (3 nm); the islands grew and coalesced as the film thickness increased.[16,17] (4) The development of quantum fortresses from the shallow indents was prevented when the fast film growth at 550 °C was interrupted by annealing at the same temperature; instead of quantum fortresses, the indents evolved into elongated trenches.[13]

The CRT formation is commonly explained by the cooperative nucleation model.[1] The model argues that the presence of one type of structure (e.g., a trench) can reduce the energy barrier for the nucleation of the other type (e.g., an island) at the adjacent site, thus facilitating the repeating occurrences of the two types of structures. The energy reduction can come from the mismatch strain in the film[1] or the adatom concentration on the film surface.[18]

The cooperative nucleation model points out the significant effects of an existing nanostructure on the nucleation of a different one. The nucleation model, however, cannot fully account for the ordered morphology and the uniform size distribution of the QDM generated by the pitted buffer layer[6] and by the fast film deposition.[11] Furthermore, nucleation requires spontaneous accumulation of a large amount of adatoms at the adjacent sites, and there is an energy barrier during the process. The difficulty in nucleating structures at the adjacent sites suggests the CRT formation may be dictated by a different mechanism.

The CRT formation is examined in this paper by considering two issues. First, instead of nucleation, the adjacent structure may develop gradually via the surface undulation process. The surface undulation process, driven by surface diffusion, is another mechanism of the morphological evolution of the film surface. The process is characterized by a

 ©2007 The American Physical Society

gradual change of the surface profile, and the process can lead to the formation of faceted islands without experiencing an energy barrier.[19–21] These unique features suggest that the surface undulation process can play an important role in the development of the adjacent structure. Second, the gradual development of the adjacent structure has to compete with the growth of the existing outermost one. The competition between the two pathways is the key to the alternative growth of ridges and trenches during the CRT formation.[22]

The two issues are studied by simulating the surface undulation process and by analyzing the energy difference between the two pathways of the CRT formation. The results confirm that the CRT formation can happen during the surface undulation process on a thick film and is caused by the competition between the two pathways. In particular, the growth of the existing outermost structure dictates the process initially when the size of the outermost structure is small. However, once the size reaches a critical value, the gradual development of a structure adjacent to the outermost one becomes the more energetically favorable pathway. The critical size differentiating the two pathways explains the alternative growth of ridges and trenches in the CRT formation. The critical size also accounts for the uniform size distribution of the ripple structures and QDMs.

The paper is organized as follows. Section II describes the model and the simulation schemes employed to study the surface undulation process driven by the surface diffusion mechanism. Section III outlines the formulas for determining the energy change due to the formation of nanostructures. Section IV shows the simulation results for the alternative growth of ridges and trenches and the formation of QDMs. Section V presents the energy analyses for the two competing pathways that cause the CRT formation. Section VI summarizes the results of this paper and discusses the limitations of the model adopted in this paper.

II. MODEL

A. Stranski-Krastanow systems

Our study is based on a continuum model for the Stranski-Krastanow (SK) system, which consists of a heteroepitaxial thin film and a thick substrate bonded coherently along a flat interface.[23–25] The film and the substrate are elastically similar materials characterized by Young's modulus E and Poisson's ratio ν. The film and the substrate are subject to a mismatch strain ϵ_0 between them, which results in deformation and strain energy in the system.[26] The strain energy is the driving force for the nanostructure formation; the characteristic strain energy density w_0 is given by $w_0=E(1+\nu)\epsilon_0^2/2(1-\nu)$.

In addition to the strain energy, the SK system is also affected by the film-substrate interaction energy and the film surface energy. The interaction accounts for the SK transition and the development of the wetting layer.[27–29] The interaction can be modeled as a special type of film surface energy of which the density g varies with the distance z between the film surface and the film substrate interface.[28] The density is given by $g(z)=g_0 l/(z+l)$ for the case where the interaction is caused by the quantum confinement and l is a material property.[29] The surface energy density γ is assumed to be a constant γ_0 except in the vicinity of the local minimums on {105}, {15 3 23}, and {113}, the facet orientations of the islands on the SiGe/Si system.[30]

The SK systems described here are characterized by two characteristic lengths, L and $\hat{g}_0 l$, given by

$$L=\frac{\gamma_0}{w_0}, \quad \hat{g}_0 l=\frac{g_0 l}{\gamma_0}. \tag{1}$$

The quantity L represents the length scale at which the strain energy reduction due to island formation is balanced by the corresponding surface energy increment. The quantity $\hat{g}_0 l$, on the other hand, is the length scale associated with the interaction energy and the surface energy.

The three parameters, L, l, and $\hat{g}_0$, are taken to be 70 nm, 0.1 nm, and 0.1, respectively, which are similar to those used in Refs. 20 and 21. The value of L is chosen to match the length scale of the $Si_{0.7}Ge_{0.3}$/Si(001) system observed in experiments,[14,16] and l and $\hat{g}_0$ are selected to capture the scenario that the $Si_{0.7}Ge_{0.3}$ film develops into separated island arrays at small film thickness.[16] The choice of L, l, and $\hat{g}_0$ has no effect on the cooperative formation at large film thickness.

B. Surface chemical potential

The thermodynamics of the film surface is determined by the surface chemical potential χ, defined as the total free energy change when one unit of the film material is bonded onto the surface of the system.[23,28,31–33] For the SK model described in the previous section, χ can be expressed as

$$\chi=\mu_0+\Omega\left[w-(g+\gamma)\kappa+\frac{\partial g}{\partial z}n_z+\nabla^\Gamma\cdot\frac{\partial\gamma}{\partial\mathbf{n}}\right], \tag{2}$$

where μ_0 is the chemical potential of the film material without stress, Ω is the atomic volume, w is the strain energy density, κ is the curvature, ∇^Γ is the surface gradient operator, and n_z is the z component of $\mathbf{n}$.

The physical meanings of the five terms in Eq. (2) are briefly discussed as follows. The first term μ_0 in Eq. (2) is the energy change when ignoring the effects of the stresses and the surface. This term is a constant when the film composition remains homogeneous. The second term Ωw is responsible for the effect that the total strain energy of the film-substrate system decreases as a flat film surface develops into a rough profile.[34–37] Hence, the second term describes an energetic force favoring surface undulation and nanostructure formation. The third term $-\Omega(g+\gamma)\kappa$ is due to a change of the surface area,[31] and evidently this term opposes the development of islanded surfaces. The fourth term accounts for the variation of the interaction energy with the film thickness,[28] and including this term is crucial for modeling the SK transition and the formation of the wetting layer. The last term is a consequence of the anisotropy of the surface energy density, determining the orientations of the facets that can form during the morphological evolution.[23,33]

C. Morphological evolution

The variation of χ on the film surface causes the morphological evolution of the system; the evolution controlled by surface diffusion is expressed as[34,38]

$$\frac{\partial f(x,y,t)}{\partial t} = \frac{\Omega \rho_s D_s}{n_z k_B T_k} \nabla^{\Gamma} \cdot (\nabla^{\Gamma} \chi), \tag{3}$$

where $f(x,y,t)$ is the film surface profile at time t, ρ_s is the adatom density, D_s is the surface diffusivity, k_B is the Boltzmann constant, and T_k is the temperature. The surface diffusion mechanism is important during the annealing as well as the growth process.

The implementation of the morphological evolution simulation was similar to those in Refs. 23–25. The simulation employed the two-dimensional (2D) Fourier series with the same wavelength in the x and y directions to describe the film surface profile $f(x,y,t)$. The wavelength of the Fourier series defined the calculation cell size, and it was taken to be $18L$ in our calculations. The simulation consisted of three basic modules for determining the evolution of the surface profile $f(x,y,t)$. The first module evaluated χ expressed in Eq. (2). In particular, the last three terms in Eq. (2) were calculated by the fast Fourier transform method, while the term w was obtained by using the high-order boundary perturbation method to solve the elasticity problem of a strained film on a thick substrate.[23] The second module then used the result χ to compute the surface migration rate $\partial f(x,y,t)/\partial t$ according to Eq. (3). Finally, the third module integrated the surface migration rate $\partial f(x,y,t)/\partial t$ with respect to time t by the generalized midpoint rule[39] to update the surface profile $f(x,y,t)$. The simulation results were normalized by the time scale $t_L = k_B T_k L^4/\rho_s D_s \Omega^2 \gamma_0$. Unless specified, the substrate orientation and thus the vertical direction are taken to be the [001] direction of the material coordinates. Our simulation lacked the capability to produce perfect facets. Nevertheless, the term facet is loosely used in this paper when describing the simulation results.

III. ENERGY OF NANOSTRUCTURES

This section summarizes the first-order boundary perturbation method for evaluating the total energy change due to the formation of strained nanostructures on the SK film-substrate system under the condition of mass conservation. For simplicity, the discussion is limited to the 2D cases, and the total energy is the sum of the strain energy and surface energy. The third type of energy in the SK system, namely, the interaction energy, can be ignored in the analyses for the CRT formation because, as demonstrated later in Sec. IV, the CRT formation occurs on thick films where the effects of the interaction energy become insignificant.

This section is divided into three parts. The first one examines the case of a single nanostructure. The second one explores the situation where an additional nanostructure develops at a site adjacent to a preexisting one. Based on the results of the second part, the third one considers the scenario that the additional adjacent structure is much smaller than the preexisting one.

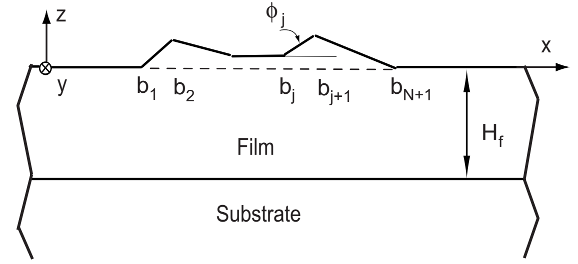

FIG. 1. Schematic diagram of a heteroepitaxial film-substrate system containing a faceted nanostructure on a flat wetting layer of thickness H_f.

A. Single nanostructure

1. System

Figure 1 depicts the morphology of a 2D strained film-substrate system that may appear during the deposition and/or annealing process. The system is attached by a set of Cartesian coordinate axes on the flat film surface. The x and y axes lie parallel with the surface, while the z axis is normal to the surface.

The substrate of the system is a semi-infinite solid, and the film consists of a flat wetting layer of thickness H_f and a nanostructure with N facets. There are totally $N+1$ vertices on the structure; the x components of the vertices are denoted as $\{b_1, b_2, \ldots, b_{N+1}\}$. The angle between the jth facet and the x direction is ϕ_j. For convenience, one of the angles, denoted as ϕ^*, is chosen to define the characteristic slope $\mathcal{S} = \tan \phi^*$ of the structure. The ratio between the slope of the jth facet and the characteristic value $\mathcal{S}$ gives the relative slope m_j of the facet, i.e., $m_j = \tan \phi_j / \mathcal{S}$.

2. Strain energy change

The strain energy change ΔW due to the formation of the nanostructure can be estimated by the first-order perturbation method, assuming the total film volume is conserved during the formation process and the slope $\mathcal{S}$ is small.[36,40,41] The starting point of the method is to determine the strain energy density $w(x)$ on the islanded film surface,[40,41]

$$w(x) = w_0^{3d} - 2 w_0 \mathcal{S} \Psi(x), \tag{4}$$

where $w_0^{3d} = 2w_0/(1+\nu)$ is the strain energy density of the flat strained film, and the function $\Psi(x)$ describes the variation of $w(x)$ on the film surface due to the nanostructure,

$$\Psi(x) = -\frac{2}{\pi} \sum_{j=1}^{N} m_j \Re \left(\ln \frac{x - b_{j+1}}{x - b_j} \right). \tag{5}$$

The symbol $\Re$ in Eq. (5) denotes the real part of a complex number. Equation (4) is accurate to the first order of $\mathcal{S}$.

The result of $w(x)$ is used in the following formula to describe the variation of the strain energy δW of the system with that of the surface profile $\delta f(x)$,[40,42,43]

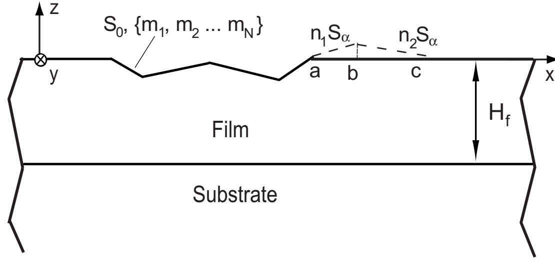

FIG. 2. Schematic diagram of a nanostructure developing at the adjacent site of a preexisting one with N facets. The adjacent structure is illustrated by the dashed line, while the preexisting one by the solid line.

$$\delta W = \int w(x)\delta f(x)dx. \tag{6}$$

Carrying out the integral in Eq. (6) and evoking the solution procedure outlined in Ref. 40 determine the strain energy change ΔW to be

$$\Delta W = - w_0 \mathcal{S} V U, \tag{7}$$

where V is the volume of the structure and U represents the effect of the nanostructure shape on ΔW,

$$U = \frac{1}{V}\int \Psi(x)f(x)dx. \tag{8}$$

The quantity U has the unique property that U remains the same when the nanostructure enlarges self-similarly.

3. Surface energy and total energy changes

The surface energy change ΔE_s due to the formation of the nanostructure can be calculated to be

$$\Delta E_s = \sum_{j=1}^{N} \gamma_0 G_j (b_{j+1} - b_j), \tag{9}$$

where $G_j = -1 + \gamma_j/(\gamma_0 \cos \phi_j)$, γ_j is the surface energy density of the jth facet, and γ_0 is that of flat film. Summing the changes of the strain and surface energy yields the total energy change ΔE_{tot},

$$\Delta E_{tot} = \Delta W + \Delta E_s. \tag{10}$$

B. Adjacent nanostructure

1. System

Figure 2 illustrates the case considered in this section where a nanostructure (denoted by the dashed line) develops at the adjacent site of a preexisting one (denoted by the solid line). The preexisting nanostructure contains N facets with the characteristic slope being $\mathcal{S}_0$; the last vertex at the right edge of the nanostructure is located at $x=a$ and $z=0$. In comparison, the adjacent nanostructure includes two surfaces. The slopes of the surfaces are $n_1\mathcal{S}_\alpha$ and $n_2\mathcal{S}_\alpha$, respectively, and $\mathcal{S}_\alpha$ is the corresponding characteristic slope. There are three vertices on the adjacent nanostructure. The first vertex is at the same location as the last vertex of the preexisting structure, the second one is at $x=b$ and $z=n_1\mathcal{S}_\alpha(b-a)$, and the third one is at $x=c$ and $z=0$.

2. Strain energy change

It follows from Eq. (4) that the strain energy density on the film surface containing the preexisting and the adjacent nanostructures can be expressed as

$$w(x) = w_0^{3d} - 2w_0\mathcal{S}_0\Psi_0(x) - 2w_0\mathcal{S}_\alpha\Psi_\alpha(x), \tag{11}$$

accurate to the first order of $\mathcal{S}_0$ and $\mathcal{S}_\alpha$. In Eq. (11), $\Psi_0(x)$ describes the variation of $w(x)$ due to the preexisting nanostructure and $\Psi_\alpha(x)$ illustrates that due to the adjacent one. Both Ψ_0 and Ψ_α can be obtained by employing Eq. (5). For example, Ψ_α can be found to be

$$\Psi_\alpha(x) = -\frac{2}{\pi}\left(n_1 \ln\frac{x-b}{x-a} + n_2 \ln\frac{x-c}{x-b}\right). \tag{12}$$

Similar to the solution procedure for deriving ΔW of a single nanostructure, Eq. (11) can be substituted into Eq. (6) to evaluate the variation of the strain energy of the system when the characteristic slope $\mathcal{S}_\alpha$ of the adjacent nanostructure increases gradually from 0 to $\mathcal{S}_\alpha$ with other parameters of the system being fixed, including $\mathcal{S}_0$ and the total mass of the film. The result can be written as[40]

$$\Delta W = - 2w_0\mathcal{S}_0 V U_0 - w_0\mathcal{S}_\alpha V U_\alpha, \tag{13}$$

where V is the volume of the adjacent nanostructure, and U_0 and U_α are given by

$$U_k = \frac{1}{V}\int \Psi_k(x)f(x)dx. \tag{14}$$

In Eq. (14), the subscript k can be 0 or α, and $f(x)$ refers to the surface profile of the adjacent nanostructure. The quantities U_0 and U_α represent the effects of the shapes of the preexisting and adjacent nanostructures on ΔW, respectively.

C. Small adjacent nanostructure with the same facet as the preexisting one

This section examines the special case where the adjacent nanostructure is small and its first facet is the same as the last one of the preexisting structure, i.e., $n_1\mathcal{S}_\alpha = m_N\mathcal{S}_0$. Since the adjacent structure is small, the function $\Psi_0(x)$ associated with the preexisting nanostructure in the vicinity of $x=a$ can be rewritten as the sum of the contribution from the vertex at $x=a$, denoted as $\Psi_a(x)$, and a constant Ψ_c representing the contribution from the remaining vertices,

$$\Psi_0(x) = \Psi_c + \Psi_a(x), \tag{15}$$

where Ψ_c and $\Psi_a(x)$ can be expressed as

$$\Psi_a(x) = -\frac{2m_N}{\pi}\ln(x-a), \tag{16}$$

$$\Psi_c = \lim_{x\to a}[\Psi_0(x) - \Psi_a(x)]. \tag{17}$$

TABLE I. The film thickness and the initial surface profiles of the three cases shown in Fig. 3.

Case	Film thickness (nm)	Initial profile
1	4	Random roughness
2	30	Random roughness
3	30	Holes and random roughness

Substituting Eqs. (12) and (15) into Eqs. (13) and (14), employing the identity $(c-b)n_2+(b-a)n_1=0$, and evoking the condition $n_1\mathcal{S}_\alpha=m_N\mathcal{S}_0$ yield ΔW for the special case considered here,

$$\Delta W = -2w_0\mathcal{S}_0\Delta V\left\{\Psi_c + \frac{m_N}{\pi}[3-2\ln(c-b)]\right\}, \quad (18)$$

where ΔV can be calculated to be

$$\Delta V = \tfrac{1}{2}\mathcal{S}_\alpha(n_1-n_2)(c-b)(b-a). \quad (19)$$

IV. NUMERICAL SIMULATION FOR THE COOPERATIVE RIDGE-TRENCH FORMATION

This section presents numerical simulation results of the CRT formation. In particular, Sec. IV A investigates the condition under which the CRT formation can be activated by the surface undulation process to produce the unique QDM morphology observed in experiments. Section IV B then examines the details of the undulation process to reveal the kinetic pathways of the CRT formation.

A. Cooperative ridge-trench formation via surface undulation

We simulated the surface undulation of three cases of $Si_{0.7}Ge_{0.3}$ films driven by the surface diffusion mechanism described in Sec. II C. The results correspond to the annealing process in experiments; the implications of the results for the growth process are discussed later in Sec. VI B.

The three cases of $Si_{0.7}Ge_{0.3}$ films had identical material properties but differed in film thickness and initial surface profiles. The two factors adopted in the three cases are summarized in Table I. In the first case the film thickness was 4 nm, which was slightly higher than the critical value for the SK transition, and the initial surface was an almost flat profile with the root-mean-square (rms) roughness being 0.05 nm. The results, depicted in Figs. 3(a1)–3(a3), and illustrated a typical example of surface undulation on a thin film with small roughness: The thin film first developed a wavy profile containing shallow bumps and valleys. The bumps then underwent shape transition from smooth structures to faceted pyramids.[19–21,44] Evidently, the surface undulation on thin films favored islands over pits and trenches.

The film morphology changed totally when the film thickness was sufficiently large. This was shown in the second case where the initial surface profile was identical but the film thickness was increased to 30 nm. Plotted in Figs. 3(b1)–3(b3), the results indicated the surface undulation process mainly resulted in faceted pits and trenches first, instead of islands or ridges. The pits and trenches subsequently facilitated the growth of pyramids and ridges at the adjacent sites, leading to a ripple structure. The ripple structure could be described as a network of nanoridges and nanotrenches. Those nanostructures were still defined by the {105} facets, while the shapes were irregular. The results agree with the experimental findings[2,3] and demonstrate that the surface undulation on thick films can cause the CRT formation.

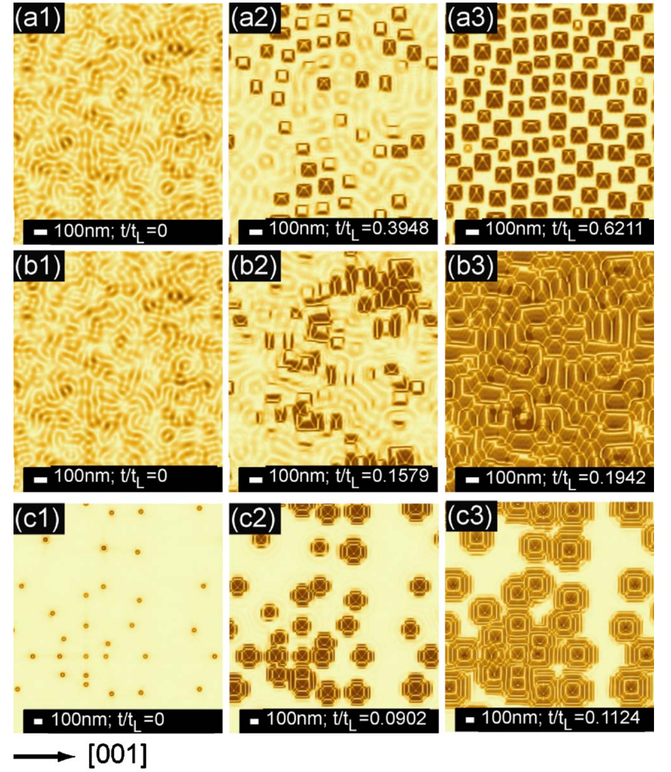

FIG. 3. (Color online) The morphological evolution of $Si_{0.7}Ge_{0.3}/Si$ with different film thicknesses and initial surface profiles. [(a1)–(a3)] $H_f=4$ nm and the initial film surface is flat with rms roughness being 0.05 nm. [(b1)–(b3)] $H_f=30$ nm and the initial profile is the same as the first case [(c1)–(c3)] $H_f=30$ nm and an array of shallow holes are present at $t=0$. The average diameter and depth of the holes are 50 and 0.9 nm, respectively. The tone of the colors represents the angle ϕ between the normal vector of the surface and the vertical direction. The lightest one corresponds to $\phi=0°$; the darkest ones to 0.14° in (a1) and (b1), 6.9° in (c1), 11.3° in (a2), (b2), (c2), and (a3), and 15° in (b3) and (c3).

Using the same film as in the second case, the third case examined how the CRT formation was affected by the presence of shallow holes on the initial surface.[45] The holes were randomly distributed; the diameter and depth of the holes were varied ±10% around the prescribed average values, which were 50 and 0.9 nm, respectively. The same random roughness as employed in the earlier cases was still included on the initial surface profile. The results, illustrated in Figs. 3(c1)–3(c3), showed that the CRT formation caused the holes to develop into QDMs of comparable shapes. The QDMs consisted of a faceted pit, a ridge ring, and a trench ring, which were consistent with the structures reported in Refs. 11 and 14. The regular QDM morphology was in con-

trast to the random distribution of trenches and ridges in the second case. The difference demonstrates the important role of shallow holes in the QDM formation.

In summary, Fig. 3 shows that the CRT formation happens on thick films; the process leads to QDMs if shallow holes are present on the initial surface and to a network of irregular ripples if the initial surface is characterized by random roughness.

The suppression of the cooperative formation on thin films can be understood as follows. Both islands and trenches and/or pits can reduce the strain energy stored in the film, and the latter is more effective than the former. Though reducing more strain energy, the formation of trenches and/or pits is obstructed on thin films because of the film-substrate interaction energy. The interaction energy favors nanostructures protruding out of the films over those penetrating into the films. Since the strength of the interaction energy increases with decreasing film thickness, the trench and/or pit growth and thus the CRT formation are impeded when H_f is small.

The significance of the interaction energy on suppressing the trench and pit formation was further investigated by employing a lower interaction energy density ($\hat{g}_0=0.01$) to simulate case 1 in Table I. The results confirmed that faceted trenches and pits formed if the interaction energy density was sufficiently low. The trenches and pits, however, exhibited flat bases at the bottom of the nanostructures instead of an apex or a sharp edge. The pit and trench shapes were different in this case because the depths of fully developed pits and trenches were larger than the thickness of the film above the wetting layer. Due to the small film thickness, when the growth of the pits and trenches approached the wetting layer, the growth was hindered by the wetting layer, leading to the formation of the flat bases.

B. Kinetic pathways

Motivated by the findings in Figs. 3(c1)–3(c3), our investigation turned to the case of a single shallow hole on a thick $Si_{0.7}Ge_{0.3}$ film to reveal the kinetic pathways of the CRT formation. The diameter and depth of the hole were 50 and 0.9 nm, respectively. In addition to the hole, the random roughness was also present on the initial surface. The morphological evolution of the hole is depicted in Figs. 4(a)–4(c). The results suggested, via the cooperative formation, the shallow hole first evolved into a QDM and then a relatively ordered ripple structure involving multiple rings of ridges and trenches. The formation process was consistent with our findings in Sec. IV A.

The formation process was further studied in Fig. 4(d) by plotting the film cross sections at different time steps along the solid line shown in Fig. 4(b). The figure reveals that the shallow hole first transformed into a faceted pit and then the pit enlarged (see lines 0–2). The pit growth was significantly impeded when ridges developed at the pit edges. The ridges were faceted on the side facing the pit initially (see line 3). Afterward, the ridges were fully faceted and grew continuously (see line 4). Similar to the pit, the ridge growth was also hindered after the ridges activated the formation of faceted trenches surrounding the ridges (see line 5). The subsequent morphological evolution on the film followed the same pattern, leading to the cooperative formation (see line 6).

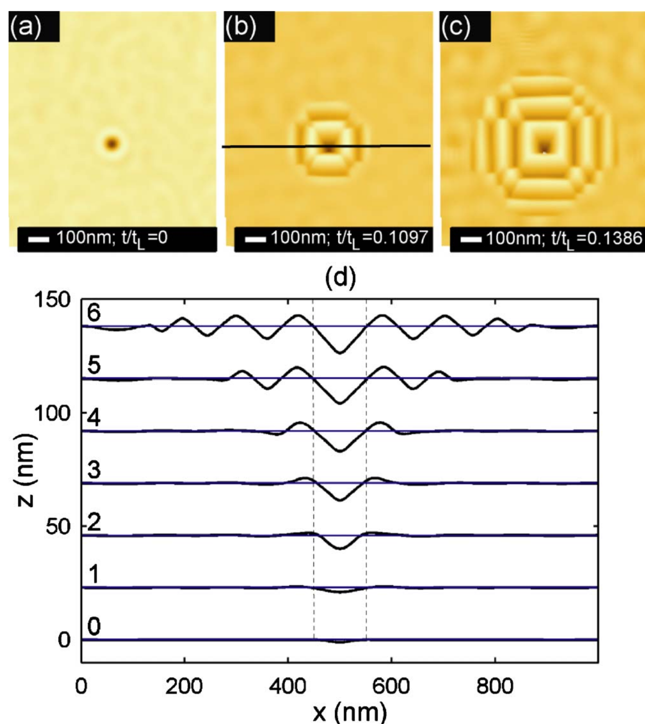

FIG. 4. (Color online) [(a)–(c)] The morphological evolution of a hole with 50 nm in diameter and 0.9 nm in depth on a film with $H_f=30$ nm. (d) The film cross sections along the solid lines shown in (b) during the evolution. In (d) the horizontal line represents the initial height of the film, and the dashed lines indicate the final pit size.

In short, Fig. 4(d) shows that the cooperative formation results from the competition of two kinetic pathways: the growth of the existing outermost nanostructure and the formation of a structure adjacent to the outermost one.

V. ENERGY ANALYSES FOR THE COOPERATIVE FORMATION

The two competing pathways of the CRT formation are analyzed from the energy point of view with the focus on the initial stage of the formation process where the shallow hole has transformed into a faceted pit. The results provide an insight into the alternative growth of ridges and trenches and the size selection mechanism of the CRT formation.

A. Model problem

Figure 5 plots the 2D model adopted in the energy analyses for the CRT formation on the surface of a heteroepitaxial film-substrate system. The film thickness is sufficiently large so that the film-substrate interaction energy in the system can be neglected, and it is the strain energy and surface energy that dictate the morphological evolution of the nanostructures on the film surface.

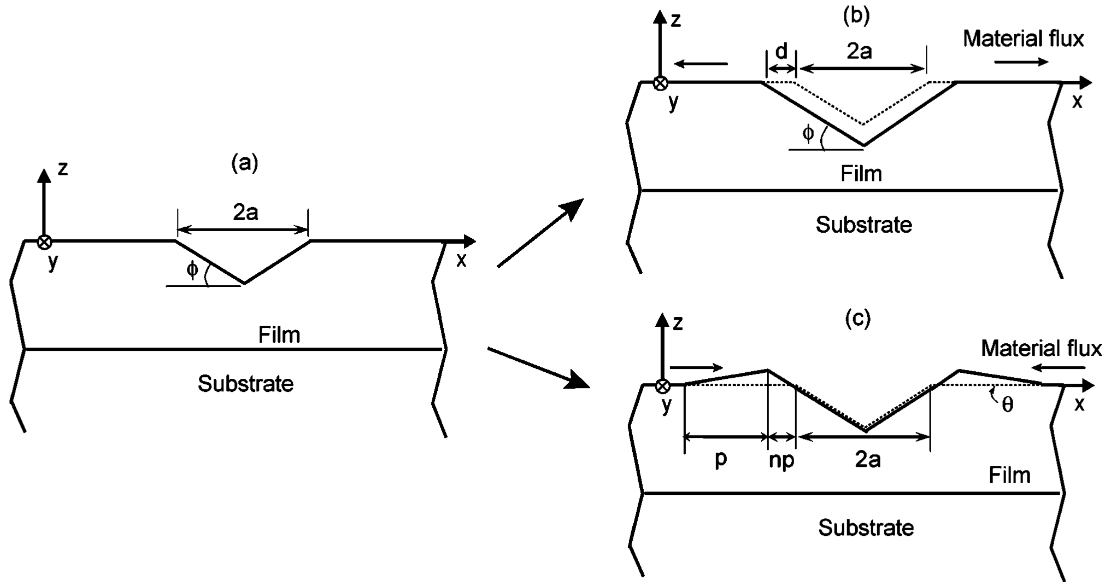

FIG. 5. Schematic diagrams of the two competing pathways of the CRT formation: (a) the initial condition, (b) the self-similar pit growth, and (c) the adjacent ridge formation. The dotted lines in (b) and (c) indicate the initial profile illustrated in (a).

The film-substrate system contains a faceted pit initially, as illustrated in Fig. 5(a). The pit may evolve via two pathways. In the first pathway, depicted in Fig. 5(b), the film material is transported from the pit surfaces to the remaining flat film profile, causing the pit to grow self-similarly. The volume ΔV (per unit length in the y direction) of the transported material can be calculated to be

$$\Delta V = \mathcal{S}(2a + d)d, \tag{20}$$

where $\mathcal{S}=\tan\phi$, ϕ is the facet angle, $2a$ is the width of the initial facet, and $2d$ is the increment of the pit width. According to Eq. (20), d can be expressed as a function of the volume ΔV,

$$d = \sqrt{a^2 + \frac{\Delta V}{\mathcal{S}}} - a. \tag{21}$$

In contrast to the first pathway, the film material in the second pathway is transported from the flat film surface to the edges of the pit, leading to the formation of a ridge at both edges of the pit, see Fig. 5(c). The surface of the ridge facing the pit is the same facet as the pit one, while the other surface of the ridge is nonfacet. The angle between the nonfacet surface and the flat film profile is θ and is allowed to vary during the formation process. The nonfacet surface with adjustable θ is adopted here as a simple model to account for the gradual ridge formation.

The surface energy density $\gamma(\theta)$ of the film surface is taken to be

$$\gamma(\theta) = \gamma_0 - \Delta\gamma \exp(-\beta|\theta - \phi|), \tag{22}$$

which contains a cusp at the facet angle $\theta=\phi$. In Eq. (22), $\Delta\gamma$ is the depth of the cusp, and $\beta\Delta\gamma$ is the gradient $d\gamma/d\theta$ at the cusp. The quantity β is assumed to be large; thus, γ approximates to γ_0 in the vicinity of $\theta=0$.

The volume ΔV of the material that is transported from the flat film surface to form the ridges can be expressed as

$$\Delta V = \mathcal{S}n(1+n)p^2, \tag{23}$$

where p, as illustrated in Fig. 5(c), is the length of the projection of the ridge nonfacet surface onto the flat film, $\mathcal{S}=\tan\phi$, and n is defined to be $n=\tan\theta/\tan\phi \approx \theta/\phi$.

The energy changes of the two pathways, namely, the self-similar pit growth and the adjacent ridge formation, are compared in the next section.

B. Energy changes

The energy change ΔE_1 due to the self-similar pit growth can be estimated by using the method discussed in Sec. III A, and the result is found to be

$$\Delta E_1 = -\frac{8\ln 2}{\pi} w_0 \mathcal{S}\Delta V + 2\gamma_0 G_\phi d, \tag{24}$$

where $G_\phi=-1+\gamma_1/\gamma_0\cos\phi$, $\gamma_1=\gamma_0-\Delta\gamma$ is the surface energy density of the facet, and d is related to ΔV by Eq. (21). In comparison, the energy change ΔE_2 due to the adjacent ridge formation is determined by adopting the scheme described in Sec. III B,

$$\Delta E_2 = -w_0 \mathcal{S}\Delta V U_2 + 2\gamma_0(nG_\phi + G_\theta)p, \tag{25}$$

where the quantity ΔVU_2 is defined in Eq. (A8) and $G_\theta=-1+\gamma(\theta)/(\gamma_0\cos\theta)$. The derivation procedure of Eqs. (24) and (25) is presented in the Appendix.

The energy difference $\Delta E=\Delta E_2-\Delta E_1$ between the ridge formation and the pit growth is illustrated in Fig. 6 by plotting the contours of ΔE as a function of ΔV and θ. The contours with $\Delta E<0$ determine the domain $(\Delta V,\theta)$ in which the adjacent ridge formation is more energetically favorable,

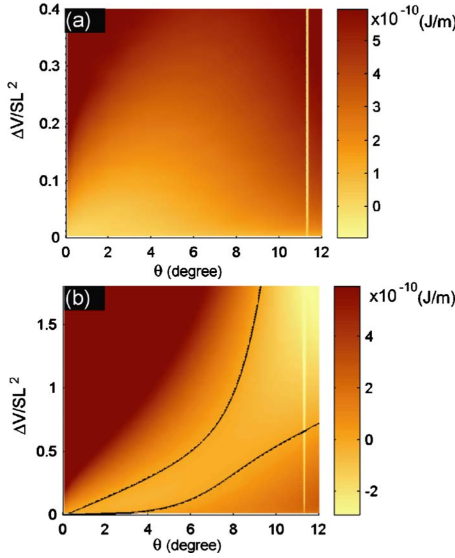

FIG. 6. (Color online) The contours of the energy difference ΔE as a function of ΔV and θ for the cases where $L=70$ nm, $\gamma_0=1$ J/m, $\Delta\gamma_0/\gamma_0=0.015$, $\phi=11.3°$, and $\beta=50$; $2a=90$ nm in (a) and $2a=190$ nm in (b).

while those with $\Delta E>0$ define the domain where the pit growth is preferred. The figure considers two cases that differ in the initial pit size: $2a=90$ and 190 nm in Figs. 6(a) and 6(b), respectively. Except a, the other parameters adopted in the two cases are identical: $L=\gamma_0/w_0=70$ nm, $\gamma_0=1$ J/m, $\Delta\gamma/\gamma_0=0.015$, $\beta=50$, and $\phi=11.3°$.

A distinctive feature in both Figs. 6(a) and 6(b) is the sharp variation of the contours in the narrow strip located at $\theta=\phi$. The narrow strip is called the facet domain in this paper since the strip corresponds to the case where the adjacent ridge is fully faceted. The remaining area, characterized by smooth contours, gives ΔE for the case where the ridge contains a nonfacet surface; this area is termed the nonfacet domain. The two domains represent different ways of adjacent ridge formation. The facet domain refers to an abrupt shape transformation, which can occur by nucleation. This domain is discussed later in Sec. V F. The nonfacet domain, in contrast, implies a gradual shape change that happens during the surface undulation process. The nonfacet domain is investigated in the following.

The nonfacet domain depicted in Fig. 6(a) shows a typical result of ΔE for the case of small pit size. The result is characterized by the pattern that ΔE is positive and increases with ΔV. The characteristic suggests the energy favors the pit growth over the adjacent ridge formation during the surface undulation process when the pit size is small.

The nonfacet domain plotted in Fig. 6(b), in contrast, represents the result of large pit size. The domain is divided into two regimes along the two black lines that depict the contours $\Delta E=0$.[46] The regime outside the two black lines indicates positive ΔE and is favored by the pit growth. The regime between the black lines, on the contrary, shows $\Delta E<0$ and is dictated by the adjacent ridge formation. The result suggests that the adjacent ridge formation can be more favorable than the pit growth during the surface undulation

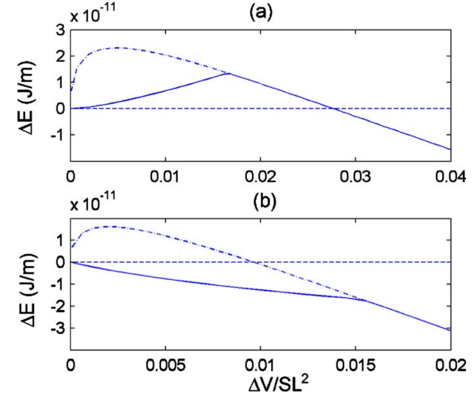

FIG. 7. (Color online) The effects of ΔV on ΔE_{eq} and ΔE of faceted ridges for the two cases shown in Fig. 6. The function ΔE_{eq} is depicted by the solid lines and ΔE of faceted ridges by the dotted-dashed lines.

process when the pit size is sufficiently large.

C. Gradient $\mathcal{F}$

The effect of the initial pit size on the adjacent ridge formation can be further understood by considering the function $\Delta E_{eq}(\Delta V)$, defined as the minimum of $\Delta E(\Delta V,\theta)$ among all θ for a given value of ΔV. The function $\Delta E_{eq}(\Delta V)$ is plotted by the solid lines in Figs. 7(a) and 7(b) for the two cases shown in Fig. 6. The two lines suggest whether the adjacent ridge formation can happen or not during the surface undulation process is determined by the gradient $\mathcal{F}$ of the function $\Delta E_{eq}(\Delta V)$ at $\Delta V=0$,

$$\mathcal{F}=\left.\frac{d\Delta E_{eq}}{d\Delta V}\right|_{\Delta V=0}. \tag{26}$$

A positive value of $\mathcal{F}$ signifies that the adjacent ridge formation encounters an energy barrier, see Fig. 7(a). On the contrary, $\mathcal{F}$ is negative if the formation process is barrierless, see Fig. 7(b).

D. Derivation of $\mathcal{F}$

The crucial quantity $\mathcal{F}$ is derived in this section. The result is then employed in the next section to determine the critical pit size for the adjacent ridge formation.

The key step in deriving $\mathcal{F}$ is to calculate ΔE_1 and ΔE_2 under the condition $\Delta V/\mathcal{S}a^2\ll 1$. For ΔE_1, the condition means d given in Eq. (21) can be expressed as $d=\Delta V/(2\mathcal{S}a)$. Applying the result to Eq. (24) yields

$$\Delta E_1=w_0\Delta V\left(-\frac{8\mathcal{S}\ln 2}{\pi}+\frac{LG_\phi}{\mathcal{S}a}\right). \tag{27}$$

For ΔE_2, the condition of small ΔV implies θ and n are small. Accordingly, $\gamma(\theta)\approx\gamma_0$, $G_\theta\ll G_\phi$, and $p=\sqrt{\Delta V/\mathcal{S}n}$. Substituting these expressions into Eq. (25), noticing that the term ΔVU_2 can be simplified by the scheme presented in Sec. III C, and ignoring the terms with higher order of n reduce ΔE_2 to

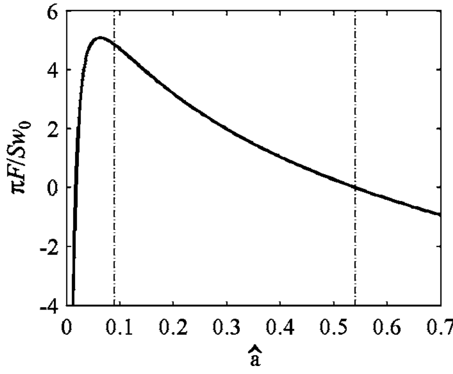

FIG. 8. The variation of $\pi\mathcal{F}/w_0\mathcal{S}$ with the normalized pit size $\hat{a}$.

$$\Delta E_2 = -\frac{w_0\mathcal{S}\Delta V}{\pi}\left[6 - 4\ln 2 + 2\ln\left(\frac{\mathcal{S}na^2}{\Delta V}\right)\right] + 2\gamma_0 G_\phi\sqrt{\frac{n\Delta V}{\mathcal{S}}}. \quad (28)$$

The derivation procedure of Eq. (28) is described in the Appendix.

The condition $\partial\Delta E_2/\partial n=0$ yields the equilibrium relative slope n_{eq} that minimizes ΔE_2 at $\Delta V/\mathcal{S}a^2 \ll 1$,

$$n_{eq} = \frac{4\mathcal{S}^3\Delta V}{\pi^2 G_\phi^2 L^2}. \quad (29)$$

Substituting Eq. (29) into Eq. (28) and subtracting ΔE_1 from the result determine the minimum ΔE_{eq} at small ΔV,

$$\Delta E_{eq} = \Delta E_2|_{n=n_{eq}} - \Delta E_1 = \frac{w_0\mathcal{S}\Delta V}{\pi}\left[-2 - \frac{\pi G_\phi L}{a\mathcal{S}^2} + 4\ln\left(\frac{4\pi G_\phi L}{a\mathcal{S}^2}\right)\right]. \quad (30)$$

Differentiating Eq. (30) with respect to ΔV gives $\mathcal{F}$,

$$\mathcal{F} = \frac{w_0\mathcal{S}}{\pi}\left(-2 - \frac{1}{4\hat{a}} - 4\ln\hat{a}\right), \quad (31)$$

where $\hat{a}$ is the normalized pit size,

$$\hat{a} = \frac{a\mathcal{S}^2}{4\pi G_\phi L}. \quad (32)$$

E. Critical pit size for adjacent ridge formation

Figure 8 plots the variation of $\pi\mathcal{F}/w_0\mathcal{S}$ with the normalized pit size $\hat{a}$. The result is divided into three ranges of $\hat{a}$: $[0,\hat{a}_{cr,0}]$, $[\hat{a}_{cr,0},\hat{a}_{cr}]$, and $[\hat{a}_{cr},\infty]$, where $\hat{a}_{cr,0}$ corresponds to the critical pit size above which the formation of the faceted pit reduces the total energy of the system,

$$\hat{a}_{cr,0} = \frac{1}{16\ln 2}, \quad (33)$$

and the quantity $\hat{a}_{cr}=0.5403$ is the larger solution of the two results that satisfy the equation $\mathcal{F}=0$.

The first range, $[0,\hat{a}_{cr,0}]$, is characterized by a drastic variation of $\mathcal{F}$. The range, however, is disregarded since the initial pit is too small to be an energetically favorable nanostructure in the first place. The second range, $[\hat{a}_{cr,0},\hat{a}_{cr}]$, is characterized by positive $\mathcal{F}$. The characteristic suggests that in the second range the pit formation is energetically favorable and the pit growth suppresses the development of adjacent ridges. The third range $[\hat{a}_{cr},\infty]$, in contrast, shows negative $\mathcal{F}$. This confirms the finding implied in Figs. 6 and 7 that the adjacent ridge formation by a gradual shape change can reduce more energy than self-similar pit growth once the pit size exceeds a critical value. By substituting $\hat{a}_{cr}=0.5403$ into Eq. (32), the critical pit size a_{cr} for the adjacent ridge formation can be expressed as

$$a_{cr} = \frac{\eta G_\phi L}{\mathcal{S}^2}, \quad (34)$$

where $\eta=4\pi\hat{a}_{cr}$. The critical value a_{cr} gives a good estimate for the pit size appearing in the cooperative formation. For example, $2a_{cr}=106$ nm for the parameters adopted in Figs. 6 and 7, which is consistent with the value reported in Ref. 11.

F. Fully faceted adjacent ridge

The adjacent ridge formation is barrierless when the ridge is allowed to change its shape during the formation process. The scenario is completely different if the adjacent ridge is fixed to be a fully faceted structure, i.e., $\theta=\phi$. The energy difference ΔE of this scenario is illustrated by the facet domain in Figs. 6(a) and 6(b) and is redrawn by the dotted-dashed lines in Figs. 7(a) and 7(b), respectively. The two dotted-dashed lines follow the same trend: ΔE increases with ΔV first, reaches a maximum, and then declines to negative values. The result demonstrates that the direct formation of a faceted structure at the adjacent site always needs to overcome an energy barrier and a critical nucleation size before the process can reduce more energy than the pit growth.

The dotted-dashed lines coincide with the solid lines in Fig. 7 after ΔV exceeds a critical value. The result shows that though the fully faceted structure is less favorable than a partially faceted one in the early stage of the adjacent ridge formation, the fully faceted one eventually becomes the most favorable morphology. The transition to the fully faceted ridge is expected to be similar to that of a single nanoisland changing from a shallow bump to a faceted pyramid.[19–21]

VI. DISCUSSION

This section first presents an overview of the CRT formation based on the results shown in Secs. IV and V. This is followed by a brief discussion on how the CRT formation may be affected by the deposition process in Sec. VI B and a survey of the limitations of the model employed in this study in Sec. VI C.

A. Cooperative ridge-trench formation

The results in Secs. IV and V reveal that the cooperative formation is an interplay between the growth of the outer-

most nanostructure and the formation of a structure adjacent to the outermost one via the surface undulation process. The cooperative formation starts with the development of faceted nanostructures on a thick film by surface undulation, a barrierless process similar to that on a thin film.[19–21] The faceted nanostructures are mainly pits and trenches.

After the faceted structure forms, the structure grows until reaching a critical size. In this stage, the growth reduces energy, and it reduces more energy than the gradual formation of adjacent structures. Above the critical size, however, the adjacent structure formation becomes more effective in reducing the energy than the growth of the first structure. As a consequence, the growth of the first structure is suppressed and the adjacent structure emerges.

The development of the adjacent structure is characterized by a sequence similar to that of the first structure: (1) formation of a small ridge with nonfacet surface, (2) shape transition to a fully faceted structure, (3) further enlargement of the structure, and (4) suppression of growth due to the formation of another adjacent structure. The repeating emergence of the adjacent structures and their self-limiting growth is the mechanism of the CRT formation.

The resulting morphology of the cooperative formation is a ripple structure consisting of nanotrenches and nanoridges. The shapes of those nanostructures are irregular if the initial surface profile is dictated by random roughness.[2,3] The nanostructures, however, can self-organize into an ordered configuration to form QDMs if the initial surface contains shallow holes.[11]

B. Deposition

Before exploring the effects of the deposition process on the CRT formation, it is helpful to discuss first how the deposition process influences the morphological evolution of the film surface from three aspects. First, the deposition introduces statistical roughening on the film surface, and this can play a crucial role in the development of shallow holes.[47] Second, the deposition increases the film thickness, which in turn influences the types of nanostructures emerging from the film surface. Third, the effects of the deposition process are controlled by the ratio between the deposition and the surface diffusion rates. The ratio can be increased by raising the deposition rate and/or reducing the substrate temperature.

Back to the effects of the deposition process on the CRT formation. Of particular interest here are the three general cases where the ratio between the deposition and the surface diffusion rates is large, moderate, and small, respectively. For the case where the ratio is large, the film can quickly become a thick one before an island array can develop. Furthermore, when the ratio is large, there is a high probability for the statistical roughening to form holes deeper than the average roughness of the film surface during the deposition process. The thick film and the holes suggest that the CRT formation happens in this case and is characterized by the development of ordered QDMs.

For the case of a moderate ratio, it is conjectured that the ratio is high enough to induce the CRT formation but insufficient to cause the statistical roughening to generate holes on the film surface. As a consequence, the film morphology is a ripple structure composed of irregular nanoridges and nanotrenches in the second case.

For the case of a small ratio, the film thickness can remain low for a long period of time to promote the development of islands on a thin wetting layer. After the development, the islands will grow in size since the material deposited onto the film surface can be transported to the islands quickly by surface diffusion. The process continues until the islands coalesce. The development and growth of the islands suppress the CRT formation in this case.

The qualitative descriptions of the three cases are consistent with the findings reported in Ref. 16. In particular, the first case of a large ratio agrees with the observations at a low deposition rate and a high temperature. The second case of a moderate ratio corresponds to the experimental results at the same deposition rate but a lower temperature. The third case of a low ratio captures the phenomenon at fast deposition and a low temperature.

C. Limitations

The surface diffusion model adopted here captures well the formation of QDMs during the fast deposition process[11,16] and the development of the ripple structure during the high-temperature annealing.[2,3] The model, however, cannot explain the finding that shallow holes evolve into long trenches when annealed at low temperatures. The difference suggests the simple model described by Eqs. (2) and (3) is suitable for the surface diffusion mechanism in the deposition and in the high-temperature annealing, while the model needs to be modified in order to simulate trench growth during annealing at low temperatures.

Besides the deposition process and the elongated trenches, other issues that need to be considered include the composition variation in the film,[48,49] the surface stress,[50] the orientation of the substrate, and the different stiffness between the film and the substrate.[51] Understanding these issues is essential for building a complete picture of the cooperative formation.

ACKNOWLEDGMENT

The project is supported by National University of Singapore (R-284-000-006-112).

APPENDIX: ENERGY CHANGES

1. Self-similar pit growth

We first consider the pit illustrated in Fig. 5(a) where the center of the pit is located at $x=0$ and the width of the pit is $2a$. Based on the information and Eq. (5), the function $\Psi_0(x)$ for the pit can be found to be

$$\Psi_0(x) = -\frac{2}{\pi}\ln\left(\frac{x^2-a^2}{x^2}\right). \tag{A1}$$

Substituting the function into Eqs. (7) and (8) yields the strain energy change W_0 due to the formation of the pit,

$$W_0 = -\frac{8 \ln 2}{\pi} w_0 \mathcal{S} V_0, \tag{A2}$$

where $V_0 = \mathcal{S}a^2$ is the pit volume. Equation (A2) suggests when the pit volume increases from V_0 to $V_0 + \Delta V$ during the self-similar growth as shown in Fig. 5(b), the total strain energy changes by

$$\Delta W_1 = -\frac{8 \ln 2}{\pi} w_0 \mathcal{S} \Delta V. \tag{A3}$$

Adding the strain energy change and the corresponding surface energy change, given by $2\gamma_0 G_\phi d$, leads to the total energy change ΔE_1 of the self-similar growth expressed in Eq. (24).

2. Adjacent ridge formation

Turn to the adjacent ridge formation illustrated in Fig. 5(c). There are two adjacent ridges in this problem, differing from that considered in Sec. III B. In spite of the difference, the strain energy change of the current case can still be calculated by Eqs. (13) and (14) presented in Sec. III B.

The calculation begins with writing down the two functions $f^-(x)$ and $f^+(x)$ that describe the shapes of the adjacent ridges at the left and right edges of the pit, respectively,

$$f^-(x) = \begin{cases} n\mathcal{S}_\alpha(x+c) & \text{for } -c < x < -b \\ -\mathcal{S}_\alpha(x+a) & \text{for } -b < x < -a, \end{cases} \tag{A4}$$

$$f^+(x) = \begin{cases} \mathcal{S}_\alpha(x-a) & \text{for } a < x < b \\ -n\mathcal{S}_\alpha(x-c) & \text{for } b < x < c, \end{cases} \tag{A5}$$

where $b = a + np$, $c = a + (n+1)p$, and $n = \tan\theta/\mathcal{S}_\alpha$. Based on the information provided in Eqs. (A4) and (A5), $\Psi_\alpha(x)$ of the two adjacent ridges can be expressed as

$$\Psi_\alpha(x) = -\frac{2}{\pi}\left(\ln\frac{x^2-b^2}{x^2-a^2} + n \ln\frac{x^2-b^2}{x-c^2}\right). \tag{A6}$$

In comparison, $\Psi_0(x)$ of the pit is given in Eq. (A1). Substituting the expressions for $\Psi_0(x)$ and $\Psi_\alpha(x)$ into Eqs. (13) and (14) and noticing that $\mathcal{S}_0$ and $\mathcal{S}_\alpha$ appearing in those two equations are equal to $\mathcal{S}$ for the current case yield the strain energy change ΔW_2 due to the adjacent ridge formation,

$$\Delta W_2 = -w_0 \mathcal{S} \Delta V U_2, \tag{A7}$$

where $\Delta V U_2$ is given by

$$\Delta V U_2 = \int_{-c}^{-a} [2\Psi_0(x) + \Psi_\alpha(x)] f^-(x) dx + \int_a^c [2\Psi_0(x) + \Psi_\alpha(x)] f^+(x) dx. \tag{A8}$$

Summing ΔW_2 and the corresponding surface energy changes yields the total energy change ΔE_2 of the adjacent ridge formation expressed in Eq. (25),

$$\Delta E_2 = -w_0 \mathcal{S} \Delta V U_2 + 2\gamma_0 (nG_\phi + G_\theta) p. \tag{A9}$$

The result is repeated here to facilitate further discussion later.

3. Infinitesimal adjacent ridges

This section focuses on ΔE_2 for the case where $\Delta V/\mathcal{S}a^2 \ll 1$, $\phi \ll 1$, and $n \ll 1$. In this special case, the strain energy change ΔW_2 can be calculated by multiplying Eq. (18) by 2,

$$\Delta W_2 = -\frac{2 w_0 \mathcal{S} \Delta V}{\pi}\left(3 - 2\ln 2 + 2 \ln\frac{a}{p}\right). \tag{A10}$$

Similarly, when $n \ll 1$ and $\phi \ll 1$, $\gamma(\theta) \approx \gamma_0$ and the quantity G_θ can be simplified to

$$G_\theta = \frac{\gamma(\theta)}{\gamma_0 \cos\theta} - 1 \approx \frac{\theta^2}{2} \approx \frac{n^2\phi^2}{2}. \tag{A11}$$

Substituting Eqs. (A10) and (A11) into Eq. (A9) and noticing that $p = \sqrt{\Delta V/\mathcal{S}n}$ at small ΔV lead to

$$\Delta E_2 = -\frac{2 w_0 \mathcal{S} \Delta V}{\pi}\left(3 - 2\ln 2 + \ln\frac{\mathcal{S}na^2}{\Delta V}\right) + 2\gamma_0 G_\phi \sqrt{\frac{n\Delta V}{\mathcal{S}}} + \gamma_0 \phi^2 \sqrt{\frac{n^3 \Delta V}{\mathcal{S}}}. \tag{A12}$$

Since $n \ll 1$ and $G_\phi > \phi^2$, the term $2\gamma_0 G_\phi \sqrt{n\Delta V/\mathcal{S}}$ in Eq. (A12) is much larger than the last term in the same equation. Consequently, the last term can be ignored, and Eq. (A12) is reduced to Eq. (28).

4. Second approach for calculating ΔW_2

In addition to the solution procedure described in Eqs. (11)–(14), the strain energy change due to the formation of an adjacent nanostructure can also be given by the difference between the strain energy of the system containing both the preexisting and the adjacent structures and that containing the preexisting one only. For the case considered in Fig. 5(c), the approach can be expressed as

$$\Delta W_2 = W_2 - W_0, \tag{A13}$$

where W_0 is given in Eq. (A2) and W_2 is the strain energy change due to the formation of the pit-ridge nanostructure.

The procedure for evaluating the quantity W_2 is similar to that for W_0, starting with the function $\Psi(x)$ for the nanostructure,

$$\Psi(x) = -\frac{2}{\pi}\left[\ln\left(\frac{x^2-b^2}{x^2}\right) - n \ln\left(\frac{x^2-c^2}{x^2-b^2}\right)\right], \tag{A14}$$

where b and c are defined in Eq. (A6). Substituting $\Psi(x)$ into Eqs. (7) and (8) leads to

$$W_2 = -w_0 \mathcal{S} \int_{-c}^{c} \Psi(x) f(x) dx, \tag{A15}$$

where $f(x)$ expresses the shape of the pit-ridge structure. The integral in Eq. (A15) is divided into four ranges, $[-c, -b]$,

$[-b,0]$, $[0,b]$, and $[b,c]$, corresponding to the four facets of the pit-ridge structure. Since the structure is symmetric, the results of the first and the second ranges are equal to those of the fourth and third ranges, respectively. Accordingly, Eq. (A15) can be reduced to

$$W_2 = -2w_0\mathcal{S}\left[\int_0^b f_3(x)\Psi(x)dx + \int_b^c f_4(x)\Psi(x)dx\right], \tag{A16}$$

where $f_3(x)=\mathcal{S}(x-a)$ describes the third facet in the range $[0,b]$, and $f_4(x)=-n\mathcal{S}(x-c)$ is for the fourth facet in $[b,c]$.

The integral in Eq. (A16) can be calculated analytically. The result, though extremely lengthy, can be significantly simplified by evoking the following Taylor series expansion under the condition $t \ll 1$:

$$\ln(1+t) = t - \frac{t^2}{2} + o(t^3). \tag{A17}$$

Deducting W_0 from the simplified expression yields the same formula given in Eq. (A10), which is derived from the solution procedure described in Eqs. (11)–(14). The agreement confirms the validity of the procedure presented in Sec. III B for determining the strain energy change due to the formation of an adjacent nanostructure.

*msecch@nus.edu.sg

[1] D. E. Jesson, K. M. Chen, S. J. Pennycook, T. Thundat, and R. J. Warmack, Phys. Rev. Lett. **77**, 1330 (1996).
[2] C. S. Ozkan, W. D. Nix, and H. Gao, Appl. Phys. Lett. **70**, 2247 (1997).
[3] C. S. Ozkan, W. D. Nix, and H. Gao, J. Mater. Res. **14**, 3247 (1999).
[4] N. S. Chokshi and J. M. Millunchick, Appl. Phys. Lett. **76**, 2382 (2000).
[5] N. Chokshi, M. Bouville, and J. M. Millunchick, J. Cryst. Growth **236**, 563 (2002).
[6] X. Deng and M. Krishnamurthy, Phys. Rev. Lett. **81**, 1473 (1998).
[7] M. Borgström, V. Zela, and W. Seifert, Nanotechnology **14**, 264 (2003).
[8] J. D. Weil, X. Deng, and M. Krishnamurthy, J. Appl. Phys. **83**, 212 (1998).
[9] R. Songmuang, S. Kiravittaya, and O. S. Schmidt, Appl. Phys. Lett. **82**, 2892 (2003).
[10] J. V. Barth, G. Costantini, and K. Kern, Nature (London) **437**, 671 (2005).
[11] J. L. Gray, R. Hull, and J. A. Floro, Appl. Phys. Lett. **81**, 2445 (2002).
[12] T. E. Vandervelde, P. Kumar, T. Kobayashi, J. L. Gray, T. Pernell, J. A. Floro, R. Hull, and J. C. Bean, Appl. Phys. Lett. **83**, 5205 (2003).
[13] J. L. Gray, R. Hull, and J. A. Floro, Appl. Phys. Lett. **85**, 3253 (2004).
[14] J. L. Gray, N. Singh, D. M. Elzey, R. Hull, and J. A. Floro, Phys. Rev. Lett. **92**, 135504 (2004).
[15] J. L. Gray, S. Atha, R. Hull, and J. A. Floro, Nano Lett. **4**, 2447 (2004).
[16] J. L. Gray, R. Hull, C.-H. Lam, P. Sutter, J. Means, and J. A. Floro, Phys. Rev. B **72**, 155323 (2005).
[17] J. A. Floro, E. Chason, R. D. Twesten, R. Q. Hwang, and L. B. Freund, Phys. Rev. Lett. **79**, 3946 (1997).
[18] M. Bouville, J. M. Millunchick, and M. L. Falk, Phys. Rev. B **70**, 235312 (2004).
[19] J. Tersoff, B. J. Spencer, A. Rastelli, and H. von Känel, Phys. Rev. Lett. **89**, 196104 (2002).
[20] C.-h. Chiu and Z. Huang, Appl. Phys. Lett. **89**, 171904 (2006).
[21] C.-h. Chiu and Z. Huang, J. Appl. Phys. **101**, 113540 (2007).
[22] Z. Huang, T. Zhou, and C.-h. Chiu, Phys. Rev. Lett. **98**, 196102 (2007).
[23] C.-h. Chiu, Appl. Phys. Lett. **75**, 3473 (1999).
[24] C.-h. Chiu, Z. Huang, and C. T. Poh, Phys. Rev. Lett. **93**, 136105 (2004).
[25] C.-h. Chiu, Phys. Rev. B **69**, 165413 (2004).
[26] H. Gao, J. Mech. Phys. Solids **42**, 741 (1994).
[27] J. Tersoff, Phys. Rev. B **43**, R9377 (1991).
[28] C.-h. Chiu and H. Gao, in *Thin Films: Stresses and Mechanical Properties V*, edited by S. P. Baker, P. Borgesen, P. H. Townsend, C. A. Ross, and C. A. Volkert (Materials Research Society, Pittsburgh, PA, 1995), p. 33.
[29] Z. Suo and Z. Zhang, Phys. Rev. B **58**, 5116 (1998).
[30] F. M. Ross, R. M. Tromp, and M. C. Reuter, Science **286**, 1931 (1999).
[31] C. Herrring, J. Appl. Phys. **21**, 437 (1950).
[32] J. R. Rice and T.-J. Chuang, J. Am. Ceram. Soc. **64**, 46 (1981).
[33] P. H. Leo and R. F. Sekerka, Acta Metall. **37**, 3119 (1989).
[34] R. J. Asaro and W. A. Tiller, Metall. Trans. **3**, 1789 (1972).
[35] D. J. Srolovitz, Acta Metall. **37**, 621 (1989).
[36] J. Tersoff and R. M. Tromp, Phys. Rev. Lett. **70**, 2782 (1993).
[37] H. Gao, Int. J. Solids Struct. **28**, 703 (1991).
[38] W. W. Mullins, J. Appl. Phys. **28**, 333 (1957).
[39] T. J. R. Hughes, *The Finite Element Method* (Prentice-Hall, Singapore, 1987).
[40] C.-h. Chiu and C. T. Poh, Phys. Rev. B **71**, 045406 (2005).
[41] I. Daruka, J. Tersoff, and A.-L. Barabási, Phys. Rev. Lett. **82**, 2753 (1999).
[42] J. D. Eshelby, in *Inelastic Behavior of Solids*, edited by M. F. Kanninen (McGraw-Hill, New York, 1970), p. 78.
[43] J. R. Rice, J. Appl. Mech. **35**, 379 (1968).
[44] A. Rastelli, H. von Känel, B. J. Spencer, and J. Tersoff, Phys. Rev. B **68**, 115301 (2003).
[45] J. L. Gray, N. Singh, D. M. Elzey, R. Hull, and J. A. Floro, Phys. Rev. Lett. **92**, 135504 (2004).
[46] The nonfacet domain of small pit size shown in Fig. 6(a) lacks the contour $\Delta E=0$ since $\Delta E>0$ in this case.
[47] C.-H. Lam, C.-K. Lee, and L. M. Sander, Phys. Rev. Lett. **89**, 216102 (2002).
[48] B. J. Spencer, P. W. Voorhees, and J. Tersoff, Phys. Rev. B **64**, 235318 (2001).
[49] Y. Tu and J. Tersoff, Phys. Rev. Lett. **98**, 096103 (2007).
[50] V. A. Shchukin, N. N. Ledentsov, P. S. Kop'ev, and D. Bimberg, Phys. Rev. Lett. **75**, 2968 (1995).
[51] B. J. Spencer, P. W. Voorhees, and S. H. Davis, Phys. Rev. Lett. **67**, 3696 (1991).